60 GHz V2I Channel Variability for Different Elevation Angle Switching Strategies

H. Groll*, E. Zöchmann*†, M. Hofer‡, H. Hammoud§, S. Sangodoyin§, T. Zemen‡,
J. Blumenstein‖, A. Prokes‖, A. F. Molisch§, C. F. Mecklenbräuker*

*Inst. of Telecommunications, TU Wien, Vienna, Austria
†Christian Doppler Laboratory for Dependable Wireless Connectivity for the Society in Motion
‡Center for Digital Safety & Security, AIT Austrian Institute of Technology, Austria
§Wireless Devices and Systems Group, University of Southern California, USA
‖Dept. of Radio Electronics, Brno University of Technology, Czech Republic
email: herbert.groll@nt.tuwien.ac.at

***Abstract*—We report results based on millimeter wave vehicle-to-infrastructure (V2I) channel measurements carried out in an urban street environment, down-town Vienna, Austria. Signal to noise ratios (SNRs) have been acquired at 60 GHz with 100 MHz bandwidth. Two horn antennas were used on a moving transmitter vehicle: one horn emitted a beam towards the horizon and the second horn emitted an elevated beam at 15-degrees up-tilt. This configuration was chosen to assess the impact of beam elevation on V2I communication channel variability. The variability of the V2I channel is shown by density estimates of the channel transfer function magnitudes. The channel changes severely along a the vehicle trajectory in an urban street scenario. Density estimates in the region with clear wide-angle view are bimodal and motivate a two-wave with diffuse power (TWDP) fading model for V2I communication with horizontal and elevated antenna beams. We compare three different strategies for beam switching: fixed, geometry-based, and SNR-based.**

***Index Terms*—millimeter wave, vehicular communications, propagation, measurements.**

I. Introduction

Vehicular communications was intensely investigated in the last decade [1]–[4]. Millimeter waves (mmWaves) have been a research topic in vehicular communications for already several decades [5], [6]. The path loss for train-to-infrastructure scenarios in the mmWave frequency band is measured in [5], performance for vehicle-to-vehicle (V2V) communication is investigated in [6].

The wide-sense stationarity of high-mobility V2I propagation was investigated based on experimental measurements in an expressway at 28 GHz [7] and the range of stationary distance is found to be 6–23 wavelengths. Simultaneous multi-band ultra wideband double-directional measurements at 6.75 GHz, 30 GHz, and 60 GHz are reported in [8]. Specifically, the propagation at a corner scenario at a "T" intersection in an urban environment was characterized by measurements, indicating that the propagation channel offers similar scattering opportunities at the sub-6 GHz and the mmWave bands.

The effect of an overtaking vehicle on a V2V channel at 60 GHz of a communicating car platoon has been investigated in [9], [10]. A more detailed statistical analysis of delay and Doppler spread is provided in [11], [12]. V2V channel measurements with antennas placed in the bumpers of cars at 38 GHz and 60 GHz, using a channel sounder with 1 GHz bandwidth, have been conducted in [13]. Further mmWave V2V measurements with approaching cars are shown in [14]. Doppler spectra of vehicle-to-infrastructure (V2I) measurements at 28 GHz in an expressway environment are shown in [15]. Doppler spectra of vibrations appearing while the vehicle is in operation are shown in [16] and [17].

Sparsity in the delay-Doppler domain for a V2I scenario at 60 GHz has been shown in [18] for a single measurement recording, and spatially agnostic characterized in [19]. The receiver SNR showed three distinct regions in terms of fading. This raises the question of probability density of the received signal strength, since the shape of a corresponding probability density function (pdf) determines the performance of a wireless receiver in the presence of noise and interference [20].

The scientific contributions in this work are descriptive statistics of the channel transfer function magnitude from the measurement campaign in [18]. The descriptive statistics show severe variability along the vehicle's trajectory in an urban street scenario. Estimates of the pdf in the region with clear wide-angle view show bimodal behavior motivating a two-wave with diffuse power (TWDP) fading model for V2I communication.

II. Measurements

The measurements took place at a crossroads in an urban street environment as shown in Figure 1. The wireless system communicates at 60 GHz with a bandwidth of 100 MHz. The transmitter (TX) antennas are 20 dBi conical horn antenna and mounted on a vehicle roof. Both horn antennas are directed in driving direction towards the crossroads. One horn emits a beam at 0° elevation angle and the second horn emits a beam at 15° elevation angle as shown in Figure 2. The receiver (RX) antenna is an omni-directional monopole antenna and mounted on a crane arm, directly above the crossroads. The thereby elevated RX antenna is at a common infrastructure height of 5 m. Each measurement recording is limited to 3600 ms

Fig. 1. V2I scenario with a transmitter vehicle approaching a receiver mounted above the street crossroads. [19]

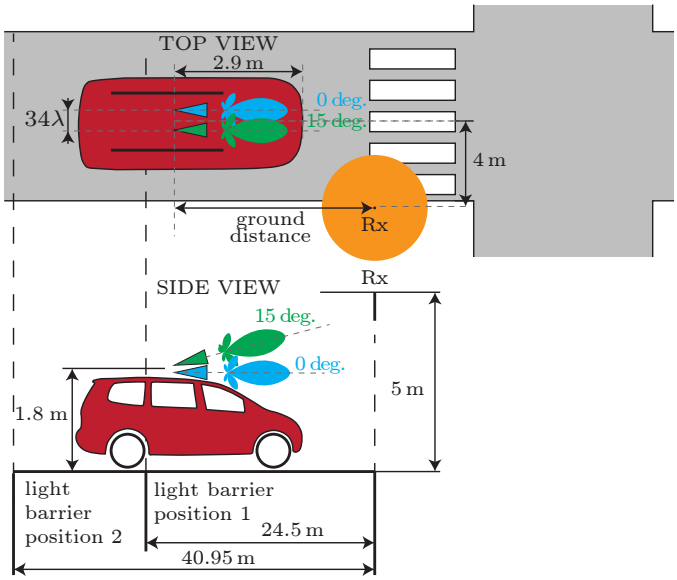

Fig. 2. Schematic of V2I scenario with distance measurements. In this work, the TX to RX ground distance is used in the investigations.

and starts at either 24.5 m or 40.95 m ground distance before the RX antenna. The data set consists of seven dual channel recordings. For more details regarding the measurement campaign, please refer to [18].

The vehicle's TX antenna ground distance to the RX antenna is derived from vision data [21]. Figure 1 shows an annotated sample frame of the vision data. This allows us to compare recordings of multiple trials on the same vehicle trajectory within a region of uncertainty.

III. Dual antenna switching strategy

The received signal sum-power to noise ratio (SNR) varies strongly over the distance covered by the vehicle as shown in Figures 3a and 3b. The SNR profile of one antenna varies only slightly among all recordings.

The V2I scenario as shown in Figures 1 and 2 allows a geometry-based TX antenna switching strategy, where the TX antenna with its beam closest to the line of sight (LOS) is selected. This selection can be made in a practical situation by the vehicle itself based on the knowledge of its and the deployed wireless infrastructure's position. In our scenario the geometric-based switching ground distance is at 24.3 m and the effective SNR is shown in Figure 3c.

Another switching strategy selects the maximum instantaneous SNR among both TX antennas, which is shown in Figure 3d. As the SNR is available at the receiver, a feedback channel is necessary for this strategy. If two transmit radio frequency (RF) chains are available, maximum ratio transmission (MRT) [22] yields an effective SNR as shown in Figure 3e.

IV. Results

The resulting SNR profiles for the different antenna switching strategies are shown in Figure 3. As already indicated in [18], three distinct fading regions due to multipath components (MPCs) are visible in the investigated scenario.

The mean of the effective SNR within a sliding window of 2 m is shown in Figure 3f. For MRT, the mean SNR is highest. However, it requires two RF chains. The maximum instantaneous SNR strategy has highest mean SNR for a switched antenna system with a single RF chain. The geometry-based strategy offers a small improvement compared to the beam with 0° elevation angle in mean SNR.

The distribution estimates of the channel transfer function's magnitudes at the LOS delay tap are shown as violin plots [23] in Figure 4 for investigated strategies. Violin plots are similar to box plots, except that they also show a kernel density estimate of the probability density at different values. 2 m windows are used to investigate the variability of the channel. The vertical dashed line marks the distance, in the direction of driving, where the 15° elevated beam is closer to the LOS compared to the 0° horizontal beam. For the geometric-based strategy, the distribution estimations are a composition of the left side of the dashed line in Figure 4a and the right side of the dashed line in Figure 4b.

Clusters of magnitudes are shown as bumps in the distribution estimates. A single peak allows for modeling the magnitudes with an unimodal pdf. A bimodal pdf has two distinct peaks and a multimodal pdf has several peaks. We observe bimodal distribution estimates for both antennas (Figures 4a and 4b) in the region from 28 to 16 meters. Within this region, the TX antennas have a clear wide-angle view to the mounted RX. The pdfs of the magnitudes become bimodal for two-wave interference and for TWDP interference with two strong distinct specular components [20] i.e. the LOS component and a ground reflection. For the horizontal beam in Figures 4a

and 4b, the region from 40 to 30 meters shows multimodal distribution estimates with at least one additional mode to possibly two modes due to the LOS component and a ground reflection One additional mode in this region is possible due to interference with MPCs scattered at the parked truck. Near the RX, the bimodal distribution vanishes and channel variability is highest between 15 and 10 meters.

The implications of the different strategies are shown in Figures 4c and 4d. The number of bimodal distribution estimates are reduced. Furthermore, the distribution estimates are more compact, especially in the region from 30 to 20 meters. Thus, the variability of the channel decreases in this region.

V. Conclusion

The variability of the investigated V2I channel is shown by density estimates of the channel transfer function magnitudes. It changes severely along a typical vehicle trajectory in an urban street scenario. The bimodal density estimates in the region with clear wide-angle view motivate the application of a TWDP fading model for V2I communication with horizontal and elevated antenna beams.

The maximum instantaneous SNR and MRT strategy offers an increase in the mean SNR and decrease the variability of the channel for regions with bimodal density estimates.

Acknowledgment

This work was supported in part by the Austrian Federal Ministry for Digital and Economic Affairs, in part by the National Foundation for Research, Technology and Development, and in part by the 5G Internet of Things – Doctoral School. The work was co-financed by the Czech Science Foundation, Project No. 17-27068S. This work was carried out in the framework of COST Action CA15104 IRACON.

References

[1] L. Cheng, B. E. Henty, D. D. Stancil, F. Bai, and P. Mudalige, "Mobile vehicle-to-vehicle narrow-band channel measurement and characterization of the 5.9 GHz dedicated short range communication (DSRC) frequency band," *IEEE Journal on Selected Areas in Communications*, vol. 25, no. 8, 2007.

[2] O. Renaudin, V.-M. Kolmonen, P. Vainikainen, and C. Oestges, "Wide-band MIMO car-to-car radio channel measurements at 5.3 GHz," in *Proc. of the IEEE 68th Vehicular Technology Conference (VTC-Fall)*, 2008.

[3] A. Paier, J. Karedal, N. Czink, C. Dumard, T. Zemen, F. Tufvesson, A. F. Molisch, and C. F. Mecklenbräuker, "Characterization of vehicle-to-vehicle radio channels from measurements at 5.2 GHz," *Wireless Personal Communications*, vol. 50, no. 1, pp. 19–32, 2009.

[4] C. F. Mecklenbräuker, A. F. Molisch, J. Karedal, F. Tufvesson, A. Paier, L. Bernadó, T. Zemen, O. Klemp, and N. Czink, "Vehicular channel characterization and its implications for wireless system design and performance," *Proceedings of the IEEE*, vol. 99, no. 7, pp. 1189–1212, 2011.

[5] H. Meinel and A. Plattner, "Millimetre-wave propagation along railway lines," *IEE Proceedings F-Communications, Radar and Signal Processing*, vol. 130, no. 7, pp. 688–694, 1983.

[6] A. Kato, K. Sato, M. Fujise, and S. Kawakami, "Propagation characteristics of 60-GHz millimeter waves for ITS inter-vehicle communications," *IEICE Transactions on Communications*, vol. 84, no. 9, pp. 2530–2539, 2001.

[7] J.-J. Park, J. Lee, K. W. Kim, M. D. Kim, H. K. Kwon, and K. C. Lee, "Wide-sense stationarity of millimeter wave expressway channels based on 28 GHz measurements," in *Proc. IEEE VTC 2019 Fall*, 2019.

[8] D. Dupleich, R. Müller, C. Schneider, S. Skoblikov, J. Luo, M. Boban, G. D. Galdo, and R. Thomä, "Multi-band vehicle to vehicle channel measurements from 6 GHz to 60 GHz at "T" intersection," in *Proc. IEEE VTC 2019 Fall*, 2019.

[9] E. Zöchmann *et al.*, "Measured delay and Doppler profiles of overtaking vehicles at 60 GHz," in *Proc. of 12th European Antennas and Propagation Conference (EuCAP)*, 2018.

[10] J. Blumenstein *et al.*, "Measured high-resolution power-delay profiles of nonstationary vehicular millimeter wave channels," in *Proc. of the IEEE 29th Annual International Symposium on Personal, Indoor and Mobile Radio Communications (PIMRC)*, 2018.

[11] E. Zöchmann *et al.*, "Statistical evaluation of delay and Doppler spread in 60 GHz vehicle-to-vehicle channels during overtaking," in *Proc. of the IEEE-APS Topical Conference on Antennas and Propagation in Wireless Communications (APWC)*, 2018.

[12] E. Zöchmann, M. Hofer, M. Lerch, S. Pratschner, L. Bernadó, J. Blumenstein, S. Caban, S. Sangodoyin, H. Groll, T. Zemen, A. Prokeš, M. Rupp, A. F. Molisch, and C. F. Mecklenbräuker, "Position-specific statistics of 60 GHz vehicular channels during overtaking," *IEEE Access*, vol. 7, pp. 14 216–14 232, 2019.

[13] M. G. Sánchez, M. P. Táboas, and E. L. Cid, "Millimeter wave radio channel characterization for 5G vehicle-to-vehicle communications," *Measurement*, vol. 95, pp. 223–229, 2017.

[14] A. Prokeš *et al.*, "Time-domain broadband 60 GHz channel sounder for vehicle-to-vehicle channel measurement," in *Proc. of the IEEE Vehicular Networking Conference (VNC)*, 2018.

[15] J.-J. Park, J. Lee, K.-W. Kim, M.-D. Kim, and K. C. Lee, "28 GHz Doppler measurements in high-speed expressway environments," in *Proc. of the IEEE 29th Annual International Symposium on Personal, Indoor and Mobile Radio Communications (PIMRC)*, 2018.

[16] A. Prokes, J. Vychodil, M. Pospisil, J. Blumenstein, T. Mikulasek, and A. Chandra, "Time-domain nonstationary intra-car channel measurement in 60 GHz band," in *Proc. of the International Conference on Advanced Technologies for Communications (ATC)*, 2016.

[17] J. Blumenstein, A. Prokes, J. Vychodil, M. Pospisil, and T. Mikulasek, "Time-varying K factor of the mm-wave vehicular channel: Velocity, vibrations and the road quality influence," in *Proc. of the IEEE 28th Annual International Symposium on Personal, Indoor, and Mobile Radio Communications (PIMRC)*, 2017.

[18] H. Groll, E. Zöchmann, S. Pratschner, M. Lerch, D. Schützenhöfer, M. Hofer, J. Blumenstein, S. Sangodoyin, T. Zemen, A. Prokes *et al.*, "Sparsity in the delay-Doppler domain for measured 60 GHz vehicle-to-infrastructure communication channels," in *2019 IEEE International Conference on Communications Workshops (ICC Workshops)*. IEEE, 2019, pp. 1–6.

[19] T. Blazek, H. Groll, S. Pratschner, and E. Zochmann, "Vehicular channel characterization in orthogonal time-frequency space," in *2019 IEEE International Conference on Communications Workshops (ICC Workshops)*, May 2019, pp. 1–5.

[20] G. D. Durgin, T. S. Rappaport, and D. A. De Wolf, "New analytical models and probability density functions for fading in wireless communications," *IEEE Transactions on Communications*, vol. 50, no. 6, pp. 1005–1015, 2002.

[21] M. Trullenque Ortiz, H. Groll, E. Zöchmann, and C. F. Mecklenbräuker, "Vehicle tracking through vision-millimeter wave Doppler shift fusion," in *Proc. of the IEEE-APS Topical Conference on Antennas and Propagation in Wireless Communications (APWC)*, 2019.

[22] T. K. Lo, "Maximum ratio transmission," in *1999 IEEE International Conference on Communications (Cat. No. 99CH36311)*, vol. 2. IEEE, 1999, pp. 1310–1314.

[23] J. L. Hintze and R. D. Nelson, "Violin plots: A box plot-density trace synergism," *The American Statistician*, vol. 52, no. 2, pp. 181–4, 1998.

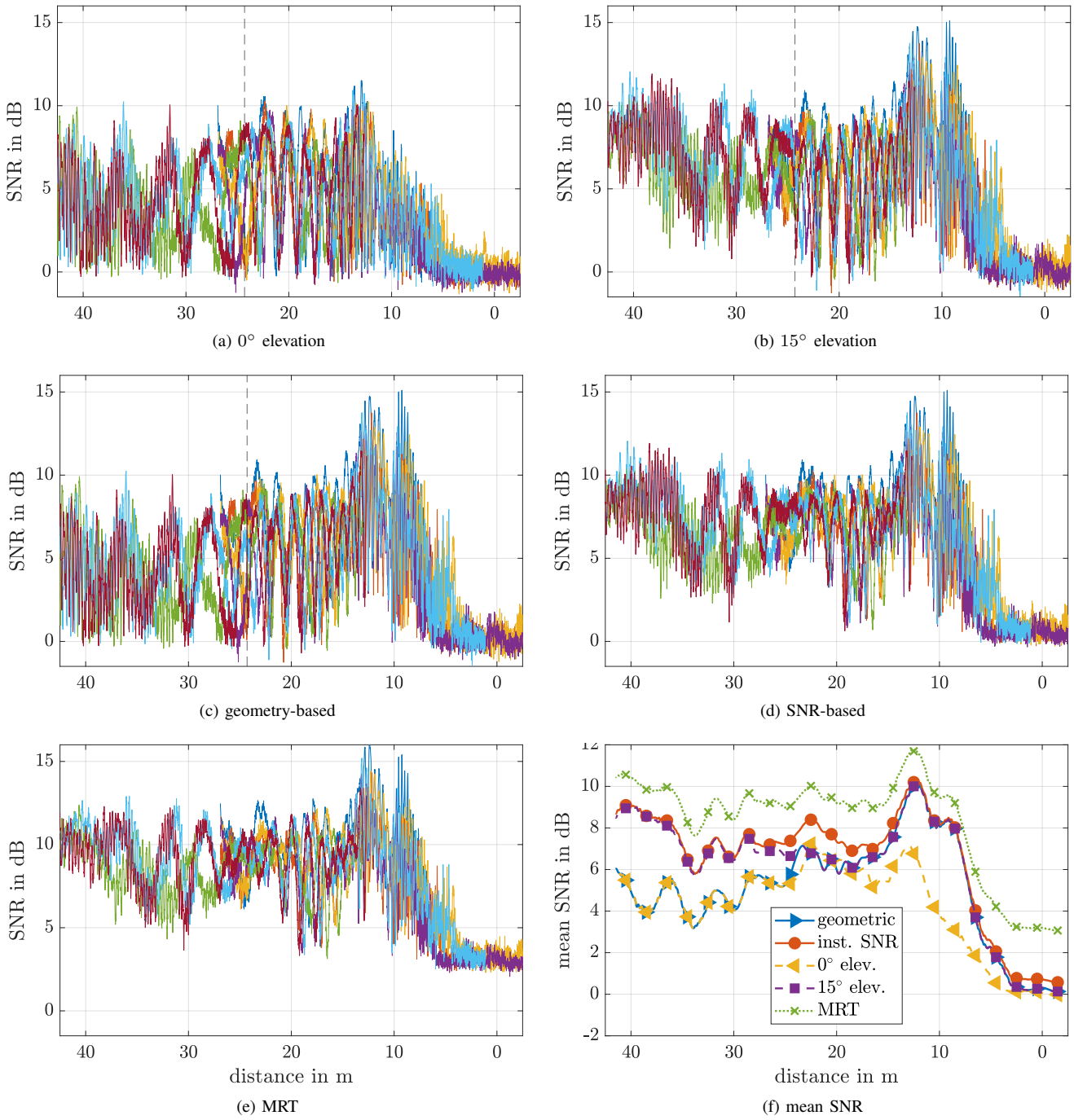

Fig. 3. (a)-(e) SNR over ground distance between TX and RX position for all measurement recordings. (f) Mean SNR within a 2 m sliding window.

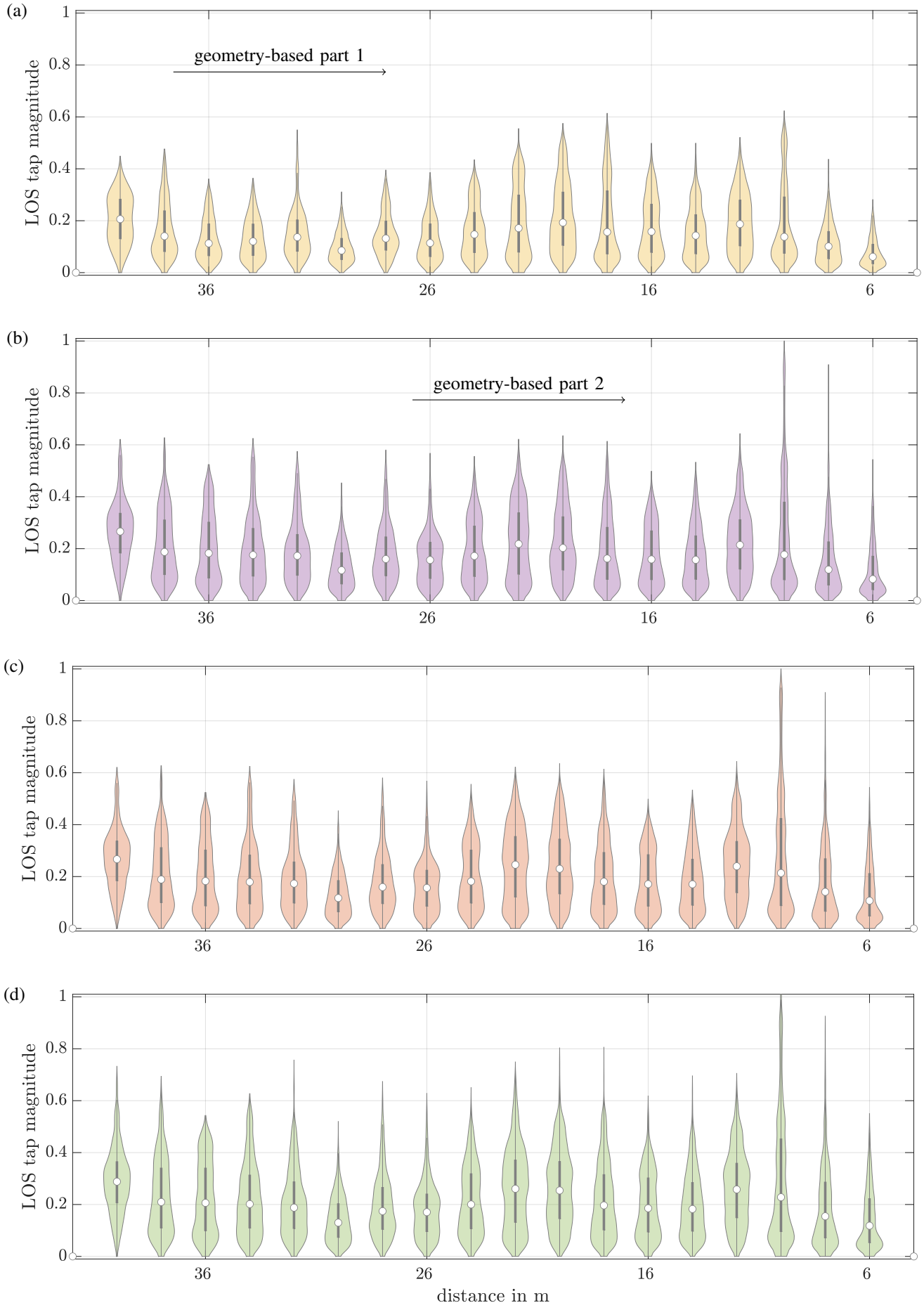

Fig. 4. Violin plots of the normalized LOS tap's magnitude within a distance of 2 m and an ensemble of 9 different trials. Circular marker indicates the median, vertical bar indicates inter-quartile range. Violin shape resembles a smoothed kernel density estimate. The geometry-based strategy is not shown, as it is easily derived from 4a and 4b